CHIN. PHYS. LETT. Vol. 34, No. 6 (2017) 066101

Compressive Behavior of TATB Grains inside TATB-Based PBX Revealed by In-Situ Neutron Diffraction *

Yi Tian(田懿)[1], Hong Wang(王虹)[1], Chang-Sheng Zhang(张昌盛)[1], Qiang Tian(田强)[1], Wei-Bin Zhang(张伟斌)[2], Hong-Jia Li(李洪佳)[1], Jian Li(李建)[1], Ben-De Liu(刘本德)[2], Guang-Ai Sun(孙光爱)[1], Tai-Ping Peng(彭太平)[1], Yao Xu(徐尧)[2**], Jian Gong(龚建)[1**]

[1]*Key Laboratory for Neutron Physics of Chinese Academy of Engineering Physics, Institute of Nuclear Physics and Chemistry, Mianyang 621900*

[2]*Institute of Chemical Materials, Mianyang 621900*

(Received 24 February 2017)

We investigate the (002) lattice strain evolution of triaminotrinitrobenzene (TATB) grains inside one TATB-based plastic bonded explosive (PBX) through the in-situ neutron diffraction. By comparing the untreated specimen with the thermal-treated one, it is found that the volume-average response of measured TATB grains remains nearly elastic during quasi-static uniaxial compression. The observed changes in TATB (002) lattice strains correlate tightly with the evolution of damage. A damage parameter defined by the macroscopically determined residual strain is further used to describe the damage degree of PBX, which suggests that the compressive behavior of TATB-based PBX is significantly influenced by the damage evolution.

PACS: 61.05.fm, 62.20.−x, 81.05.−t DOI: 10.1088/0256-307X/34/6/066101

Triaminotrinitrobenzene (TATB) is an anisotropic molecular crystal with graphite-like layered crystal structure.[1] Generally, TATB and other explosive grains are mixed with polymeric binders (5–10 wt.%) to produce plastic bonded explosives (PBXs).[2] During their working life, PBXs are subject to various loadings, which induce the micro-fracturing process within them. The growth of micro-fractures can damage the PBXs and can lead to their final failure. The investigation of damage is therefore important for the mechanical behavior and the safety use of PBX. Through the ex-situ microscopy investigation, it has been observed that the dominating damage in Brazilian test is interfacial debonding, which is randomly generated at the boundary of particles and propagates along it.[3] A similar phenomenon in compression with more particle fractures has also been observed by Chen *et al.*[4] Through the Moiré interferometry, Rae *et al.*[5] have found that the contours of the surficial displacement map are concentrated around the cracks. Liu *et al.*[6] have demonstrated that the damage reveals itself as the stress concentration in the strain field obtained by the digital image correlation (DIC) technique. Ellis *et al.*[7] have attempted to link the global damage accumulation to the mechanical behavior of PBX by the in-situ acoustic emission (AE) technique. By combining AE with DIC, Wang *et al.*[8] have investigated that the changes in homogeneity of the strain field are correlated to the damage evolution. Current reports mostly focus on the correlation between the damage evolution and the surficial deformation of PBX. However, the influence of damage evolution on the mechanical behavior of explosive grains inside the PBX also deserves attention. This study monitors directly and quantitatively the internal strain of explosive grains inside the PBX during quasi-static uniaxial compression, by combining the advantages of the large penetration depth and the in-situ observation of neutron diffraction.

The specimens were TATB-based PBXs. The averaged particle size of TATB grains was approximately 16 μm with the crest value of 19 μm.[9] The specimens were cut from the original PBX, with the diameter of 10 mm and length of 15 mm. For the purpose of comparative study, a thermal-treated specimen was also investigated, which shows the better mechanical properties. The heat treatment was carried out in a self-controlled oven at 150℃. The in-situ neutron diffraction experiments were performed at ambient temperature (∼25℃) on the residual stress neutron diffractometer (RSND) at China Mianyang Research Reactor (CMRR).[10] A Deben 2 kN dual leadscrew loading stage was installed on the sample stage. The specimen was fixed horizontally between two customized loading fixtures. Before each experiment, a small pre-load (nominally 3 N) was applied to keep the specimens in place. The motor speed was set as 0.05 mm/min in the stress control mode. The wavelength λ of the neutron beam was chosen to be 0.1587 nm for the maximum flux. The diffraction angle 2θ was set as 29° so that (002) lattice planes of TATB grains normal to the compressive direction were measured. The gauge volume of $4\times4\times8\,\mathrm{mm}^3$ in the centroid of the specimen was used for the diffraction measurement, as shown in Fig. 1. Under this layout, the (002) lattice strain evolution during the monotonic and cyclic compression was respectively measured for the untreated and thermal-treated specimens.

The lattice strain can be formulated as[11]

$$\varepsilon_{hkl} = (d_{hkl} - d^0_{hkl})/d^0_{hkl} = -\cot(\theta_{hkl})\Delta\theta_{hkl}, \quad (1)$$

where ε_{hkl} and d_{hkl} are, respectively, the lattice strain

*Supported by the National Natural Science Foundation of China under Grant Nos 51231002 and 51501170, and the President Foundation of the China Academy of Engineering Physics under Grant No 20141024.

**Corresponding author. Email: xuyao@caep.cn; gongjian@caep.cn

© 2017 Chinese Physical Society and IOP Publishing Ltd

and the interplanar distance for the selected (hkl) lattice plane of the strained specimen, d^0_{hkl} is the interplanar distance of the strain-free specimen, θ_{hkl} is the peak position obtained from the fitting curves, and $\Delta\theta_{hkl}$ is the shift of peak positions between the strained and strain-free specimens. The obtained (002) peak positions 2θ for the untreated and thermal-treated specimens during the monotonic and cyclic compression are listed in Table 1. The (002) peak positions measured at 0 MPa are set as the reference positions.

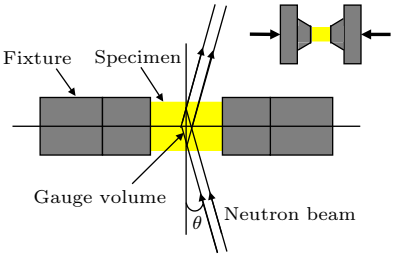


Fig. 1. Schematic diagram of the in-situ neutron diffraction experiment. The inset shows the front view of specimen and fixtures.

Table 1. The values of 2θ of the untreated and thermal-treated specimens at and unloaded from different applied stresses.

Untreated specimen				Thermal-treated specimen			
Applied stress (MPa)	2θ (deg) ±0.002	Unloaded stress (MPa)	2θ (deg) ±0.002	Applied stress (MPa)	2θ (deg) ±0.003	Unloaded stress (MPa)	2θ (deg) ±0.003
0.0	29.078	0.0	29.079	0.0	29.084	0.0	29.087
3.0	29.092	3.0	29.079	4.0	29.090[a]	5.4	29.099[a]
6.0	29.099	6.0	29.082	8.0	29.106	8.0	29.100
9.0	29.098	9.0	29.089	12.0	29.121[b]	12.0	29.101
12.0	29.111	12.0	29.080	16.0	29.131	16.0	29.084
14.0	29.108	13.6	29.081	20.0	29.134	20.0	29.107
				23.7	29.148	24.0	29.097[a]
				24.9	29.141		

[a]The standard error is 0.004°, and [b]the standard error is 0.002°.

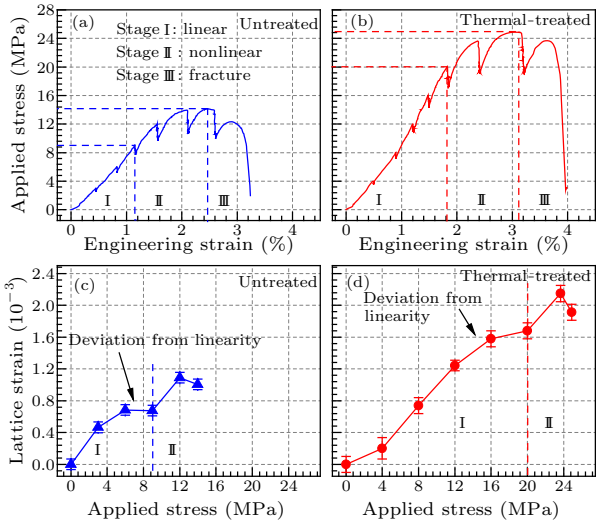


Fig. 2. Experimental data obtained during the monotonic compression: macroscopic stress–strain curves of (a) untreated and (b) thermal-treated specimens, (002) lattice strains of (c) untreated and (d) thermal-treated specimens.

Typical macroscopic stress–strain curves for the untreated and thermal-treated specimens during the monotonic compression are shown in Figs. 2(a) and 2(b), respectively. For simplicity, the obtained compressive stress and strain data have been expressed as positive quantities. The stress versus strain curves contain several dropping steps caused by some stress releasing during the diffraction measurement. Compared with the untreated specimen, the thermal-treated one exhibits noticeably better compressive properties, with the increase of the elastic modulus, yield strength, maximum strength and maximum strain. The yield point of specimens was determined by differentiating the stress–strain curves from the ex-situ compression. However, strictly distinguishing between the linear and nonlinear parts is not evident due to the viscous properties of PBX. According to the maximum strength and the measuring point near the yield point, the stress–strain curve can be roughly divided into three stages, as marked on the graph. Stage I is the linear part of the curve, which represents the elastic deformation of the specimen. This stage is slightly concave due to the densification of specimen. Then, the decline of the curve slope begins to speed up, marked as stage Ⅱ. This stage represents the plastic deformation of the specimen. The top of the curve marks the beginning of stage Ⅲ. During this stage, the unloading process happens due to the failure of the specimen.

The (002) lattice strains plotted as a function of the applied stress for the two specimens are shown in Figs. 2(c) and 2(d), respectively. During the stage I, the evolution of (002) lattice strain appears as a tensile deviation from linearity. The tensile deviation indicates that less stress is taken up by TATB grains with increasing the applied stress. Once the nonlinear behavior happens, the evolution of (002) lattice strain begins to shift towards compression, indicating that there is a load transferring back to TATB grains. The decrease at last is caused by the large stress releasing. The tensile deviation and compressive shift appear at different lattice strains in the two curves, respectively, indicating that the thermal treatment on specimens can retard their appearance. In consideration of the excellent thermal stability of TATB grains,[12] two different damage processes should be responsible for these two changes in the evolution of (002) lattice strain. Therefore, the volume-averaged response of measured TATB grains remains nearly elastic during the compression. It can be inferred that the damage process causing the curve shifting towards com-

pression also contributes to the nonlinear behavior of specimens.

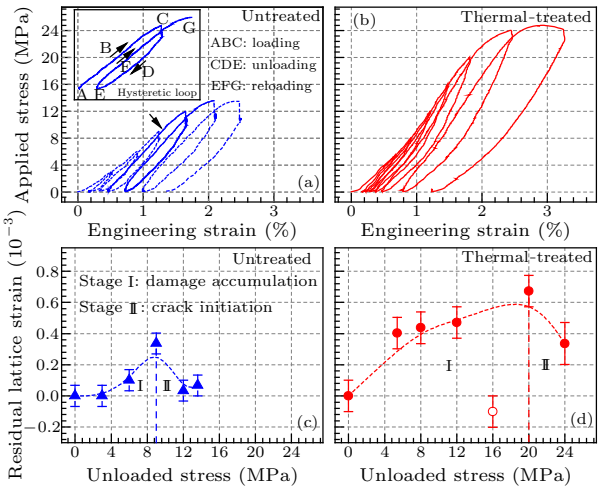


Fig. 3. Experimental data obtained during the cyclic compression: macroscopic stress–strain curves of (a) untreated and (b) thermal-treated specimens, residual (002) lattice strains of (c) untreated and (d) thermal-treated specimens.

Typical macroscopic stress–strain curves for the untreated and thermal-treated specimens during the cyclic compression are shown in Figs. 3(a) and 3(b), respectively. The specimens were loaded to the set stress and then unloaded to zero for diffraction measurement. The fixtures never return to their original location when the applied stress is completely removed. The irreversible deformation generated during the loading process remains to be the residual strain. The residual strain increases steadily during the stage I, and begins to speed up when reaching the stage Ⅱ. Due to the difference between the loading and unloading curves, a hysteresis loop is formed as marked on the graph. This hysteretic behavior contributes to the internal slippage.[13] At the initial load, TATB grains and the binder deform elastic. Then, the inhomogeneous deformation promotes the relative slippage between TATB grains. Therefore, the slope of loading curve decreases before reaching the set point. When the unloading process starts, the elastic deformation of TATB grains and the binder vanishes first. Thus the initial modulus of the unloading curve is different from the upper part of the loading curve. Once the elastic deformation disappears, the release of applied stress which balances the slippage causes it to begin in the opposite direction.[14] The modulus of the unloading curve decreases accordingly. When the applied stress is removed, the irreversible deformation adds to the residual strain. During the reloading process, the increased applied stress will cause more slippage leading to a larger residual strain.

The (002) lattice strains for the untreated and thermal-treated specimens during the cyclic compression when the applied stress is removed are shown in Figs. 3(c) and (d), respectively. Similarly, the evolution of residual (002) lattice strain can be divided into two stages. During the stage I, the residual (002) lattice strain increases with the unloaded stress, which correlates to the increase in slippage. The relative slippage between TATB gains induces the tensile stress concentration at the particle/matrix interface, and causes some tensile plastic deformation. When the applied stress is removed, the plastic deformation generates tensile residual strain at the interface. Consequently, some compressive residual strain remains in TATB grains due to the force equilibrium. Despite the linear increase of the residual strain, the residual (002) lattice strain does not increase steadily. This nonlinear increase suggests that some microdamage such as small interfacial debonding generates along with the plastic deformation, which releases a part of the residual (002) lattice strain after each cycle.[15] The generation of damage is stable during the stage I, and is therefore described as the damage accumulation. When unloaded from the stage Ⅱ, the residual (002) lattice strain decreases, indicating that some cracks are formed inside the specimen. The crack initiation and propagation destruct the structure of specimen, causing the nonlinear behavior of the specimen. It is noted that there appears a strange point for the thermal-treated specimen, as marked with the open circle on the graph, which was also observed in another repeated experiment. In consideration of the inherent residual stress, the strange point should represent a stress-free state generated before the stage Ⅱ. The mechanism behind it remains an open question, but it seems to be in connection with the transform from continuum damage to local damage. The strengths of particle/matrix interfaces inside the thermal-treated specimen are more homogeneous. Once the applied stress reaches their ultimate, 16 MPa for instance, most of the particle/matrix interfaces might have small interface debonding simultaneously. The residual (002) lattice strain will be released since there are free surfaces along every TATB grain. During the next cycle, the crack initiation starts at the beginning of the stage Ⅱ. The small interface debonding along the major tensile stress concentration will grow to a small crack while the others will disappear.[16] With the decline of free surface, the residual (002) lattice strain increases again, and decreases subsequently due to the crack propagation during the stage Ⅱ. Without the effect of the thermal treatment, the generation of small interface debonding is probably too dispersed to be observed in the untreated specimen.

Accordingly, the tensile deviation of (002) lattice strain observed during the monotonic compression is caused by the relative slippage between TATB grains. Some of the increasing applied stresses are balanced by the tensile stress generated at the particle/matrix interface. Once the crack initiation starts, due to the release of the tensile stress, more increasing applied stresses are then taken up by TATB grains. The evolution of (002) lattice strain shifts towards compression. The changes observed in (002) lattice strain evolution reflect the bulk influence of the damage evolution on it. To link the damage evolution to the mechanical behavior of specimens, it is necessary to define a

parameter to describe the damage degree during the compression. Since the elastic modulus does not show a steady decline during the cyclic compression, the residual strains is used to define the damage parameter instead,[17] which is formulated as

$$D = \frac{\varepsilon_{\mathrm{r}}^{i}}{\varepsilon_{\mathrm{r_max}}}, \tag{2}$$

where $\varepsilon_{\mathrm{r}}^{i}$ is the residual strain of the ith cycle, and $\varepsilon_{\mathrm{r_max}}$ is the residual strain when unloaded from the maximum stress. The specimen will reach its maximum strength when $D = 1$. The damage parameter D is plotted as a function of the applied stress as shown in Fig. 4(a). The contribution of contact adjustment between specimen and fixtures at the start of the load is deducted. The damage parameter increases steadily during the damage accumulation, and begins to speed up when the crack initiation starts. Disregarding the deviations caused by measurement intervals and initial damage degree, the nonlinear behavior of the thermal-treated and untreated specimens almost appear at a similar damage parameter, as marked with a dashed line on the graph. It can be inferred that the damage evolution has a significant influence on the compressive behavior of specimens, along with the applied stress affecting the generation of damage. When the damage accumulation approaches its ultimate value, the crack initiation starts and causes the nonlinear behavior of specimens.

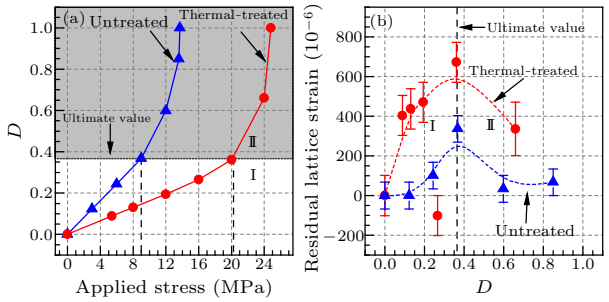


Fig. 4. (a) The evolution of damage parameter plotted as a function of the applied stress. (b) Changes in residual (002) lattice strains plotted as a function of the damage parameter.

Moreover, the residual (002) lattice strain obtained during the cyclic compression is plotted as a function of the damage parameter as shown in Fig. 4(b). The corresponding ultimate value is marked with a dashed line on the graph. Both of the curves show a similar tendency subject to the damage parameter. At the same damage parameter, the residual (002) lattice strain of the thermal treated specimen is larger than the untreated one. It seems that the generation of small interface debonding in the untreated specimen is much easier, which means that the thermal treatment is capable of strengthening the particle/matrix interface. There are several possible effects of the thermal treatment on the specimens. First, the motion of molecular chains of the binder will be enhanced during the thermal treatment. Their arrangement will be more regular so that the crystallinity of the binder has a tendency to increase. The elastic modulus of the thermal-treated specimen becomes larger consequently. Secondly, the melting temperature T_{m} of the binder is well below the heating temperature here.[18] During the thermal treatment, the melting binder will improve its adhesion to TATB grains, release part of residual stress and repair some defects. The internal quality of the thermal-treated specimen will be more continuous and homogeneous making it capable of bearing larger applied stress.

In summary, the (002) lattice strain of TATB grains inside one TATB-based PBX during the compression has been measured by the in-situ neutron diffraction. The comparison between the untreated and thermal-treated specimens indicates that the volume-averaged response of measured TATB grains remains nearly elastic. During the linear behavior of specimen, the tensile deviation of (002) lattice strain is caused by the relative slippage between TATB grains. The residual (002) lattice strain is caused by the resulting tensile residual strain and is subject to the damage accumulation. The crack initiation, which is responsible for the nonlinear behavior of specimens, starts when the damage accumulation reaches the ultimate value. The crack initiation causes the (002) lattice strain to shift towards compression, and makes the residual (002) lattice strain decrease. The damage evolution has a significant influence on the compressive behavior of specimens.

References

[1] Cady H H and Larson A C 1965 *Acta Crystallogr.* **18** 485
[2] Yan Q L, Zeman S and Elbeih A 2012 *Thermochim. Acta* **537** 1
[3] Rae P J, Goldrein H T, Palmer S J P, Field J E and Lewis A L 2002 *Proc. R. Soc. London Ser.* A **458** 743
[4] Zhou Z, Chen P, Duan Z and Huang F 2012 *Strain* **48** 326
[5] Rae P J, Palmer S J P, Goldrein H T, Field J E and Lewis A L 2002 *Proc. R. Soc. London Ser.* A **458** 2227
[6] Liu Z W, Xie H M, Li K X, Chen P W and Huang F L 2009 *Polym. Test.* **28** 627
[7] Ellis K, Leppard C and Radesk H 2005 *J. Mater. Sci.* **40** 6241
[8] Wang X, Ma S P, Zhao Y T, Zhou Z B and Chen P W 2011 *Polym. Test.* **30** 861
[9] Song H J 2000 *PhD Dissertation* (Mianyang: China Academy of Engineering Physics) (in Chinese)
[10] Li J, Wang H, Sun G A, Chen B, Chen Y Z and Pang B B 2015 *Nucl. Instrum. Methods Phys. Res. Sect.* A **783** 76
[11] Hutchings M T, Withers P J, Holden T M and Lorentzen T 2005 *Introduction Characterization Residual Stress By Neutron Diffraction* (US: CRC Press) chap 3 p 84
[12] Boddu V M, Viswanath D S, Ghosh T K and Damavarapu R 2010 *J. Hazard. Mater.* **181** 1
[13] Chen L, Han D, Bai S L, Zhao F and Chen J K 2016 *Mech. Adv. Mater. Struc.* (in press)
[14] Poon B, Ponson L, Zhao J and Ravichandran G 2011 *J. Mech. Phys. Solids* **59** 2238
[15] Oliver E C, Daymond M R and Withers P J 2004 *Acta Mater.* **52** 1937
[16] Tan H, Liu C, Huang Y and Geubelle P H 2005 *J. Mech. Phys. Solids* **53** 1892
[17] Eberhardt E, Stead D and Stimpson B 1999 *Int. J. Rock Mech. Min.* **36** 361
[18] Liu J L, Wang X C and Sun J 2007 *Eng. Plast. Appl.* **35** 54 (in Chinese)